Spatial–Temporal Structures of Trend and Oscillatory Variabilities of Precipitation over Northern Eurasia

XIAOLAN L. WANG AND HAN-RU CHO

Department of Physics, University of Toronto, Toronto, Ontario, Canada

(Manuscript received 29 April 1996, in final form 10 February 1997)

ABSTRACT

Combinations of statistical analyses including principal component analysis, and uni- and multivariate singular spectrum analyses, were carried out to characterize the spatial–temporal structures of trend and interannual oscillatory variabilities of precipitation over the major north-flowing river basins in the former Soviet Union.

The series of monthly precipitation were corrected for the biases of precipitation measurement due to the gauge-type change and changes in observing procedures. An upward trend was found in the monthly precipitation series for the last half century. This upward trend was stronger in the North Dvina and Pechora River basins, and in the Ob-Irtysh River basins, but much weaker (still upward, though) in the Yenisey–Lena River basins. The notable increases of precipitation over the southwestern part—the Volga and Ural River basins—were found to be due at least in part to the upward phase of some quasi-century periodicity. Generally speaking, the precipitation increases appeared to be more apparent during the cold seasons in the western half of the sector, while in the eastern part, it appeared to be equally or more notable during summer.

On the interannual timescales, signals of 4–5-yr and quasi-biennial oscillations were found in the space–time-dependent precipitation series. The 4–5-yr oscillation was quite apparent over the entire Northern Eurasian sector, being stronger over the southeastern and western parts. This oscillation appeared to propagate eastward. The quasi-biennial oscillation was generally weaker; it was very weak during the 1955–65 period. This oscillation was relatively stronger in the western half of the sector and weaker over the eastern half.

1. Introduction

The north-flowing runoff in Eurasia and North America may play a part in regulating the global thermohaline circulation through the hydrological cycle of the Arctic Ocean. According to Table 1 of Barry et al. (1993), the continental runoff amounts to about 53.9% of the total freshwater (freshwater fractions are relative to 34.80 salinity) into the Arctic Ocean, more than the joint contributions of the Bering Strait inflow (approx. 27.3%), Arctic net precipitation (approx. 14.7%), and import with Norwegian Coastal Current (approx. 4.1%). Of the total annual runoff of about 3300 km^3, the largest contribution (about 1650 $km^3\ yr^{-1}$) enters the Eurasian shelf seas, particularly from the Ob, Yenisey, and Lena Rivers in Siberia, with a further 340 $km^3\ yr^{-1}$ from the Mackenzie River (Barry et al. 1993). The major transport of freshwater out of the Arctic Basin is via ice discharge through the Fram Strait (north of the Greenland Sea). Such Arctic freshwater outflow into the North Atlantic exerts regulating effects on the thermohaline circulation in the ocean.

The thermohaline circulation plays an important role in the formation and variation of the earth's climate; it is sensitive to the amount of freshwater input to the North Atlantic Ocean. The heating by the thermohaline circulation makes the northern North Atlantic about 4°C warmer than the corresponding latitudes in the Pacific and is responsible for the mild climate of Western Europe (Rahmstorf 1995). Clearly, then, any change of this circulation would have considerable effects on the climate of the North Atlantic region. In the present climate, high-latitude cooling together with low-latitude heating accelerates the thermohaline circulation with poleward flow at surface, while high-latitude precipitation, runoff and ice melt, and low-latitude evaporation tend to slow it down (Weaver 1995). Using the results from a global ocean circulation model coupled to a simplified model atmosphere, Rahmstorf (1995) suggests that a continual $0.06 \times 10^6\ m^3\ s^{-1}$ of additional freshwater into the North Atlantic could *irreversibly* shut down the thermohaline circulation, with a pronounced cooling effect on the surrounding areas. Therefore, changes in the continental runoff from Northern Eurasia, which themselves could be the consequence of anthropogenic climate change, could influence the Arc-

Corresponding author address: Dr. Xiaolan Wang, Canadian Centre for Climate Modelling and Analysis, Atmospheric Environment Service, University of Victoria, P.O. Box 1700, MS 3339, Victoria, BC V8W 2Y2, Canada.
E-mail: Xiaolan.Wang@ec.gc.ca

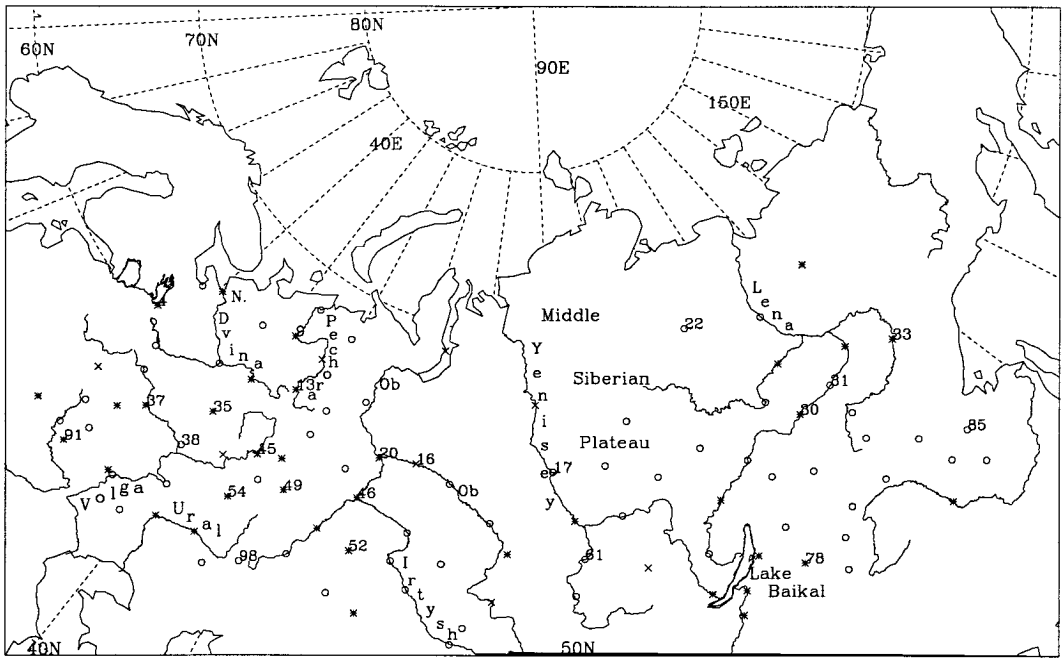

FIG. 1. Locations of major rivers and the 102 stations in the Northern Eurasian sector with daily precipitation records. Stations marked by an asterisk have records for at least 90 yr. Stations marked by a cross have records beginning later than Jan 1939 or ending earlier than Dec 1989.

tic Ocean hydrological cycle, and hence the global thermohaline circulation and the climate of the earth. On the other hand, recent results from coupled atmosphere–ocean modeling aimed at understanding the climate response to increasing greenhouse gases have all shown that, as the climate warms, the northward transport of water vapor in the atmosphere is enhanced, thereby increasing the supply of freshwater to the North Atlantic Ocean (Weaver 1995). Consistent with this is the fact that a notable upward trend has been found in the area-averaged precipitation over the former Soviet Union (37°–70°N, 25°–140°E) during the last century, and this upward trend of precipitation has remained notable, unchanged by the corrections of biases of precipitation measurement (Houghton et al. 1992; Groisman et al. 1991; Groisman 1991; Vinnikov et al. 1990; Diaz et al. 1989; Bradley et al. 1987).

The main goal of this study is to investigate large-scale spatial–temporal structures of trend and oscillatory variabilities of precipitation over the major north-flowing river basins in the former Soviet Union. Long-term records of monthly precipitation amounts from 102 stations over the northern Eurasian sector (35°–135°E, 50°–70°N) of the former Soviet Union were analyzed: slower-than-annual variations were extracted and delineated by means of singular spectrum analysis combined with maximum entropy spectrum analysis and the Kendall test of randomness. Following a description of the dataset and the strategy in section 2, most dominant spatial patterns (spatial-empirical orthogonal functions, S-EOFs) of precipitation are presented in section 3, together with the low-frequency (slower-than-annual) components of the associated spatial-principal components (S-PCs). The spatial–temporal structures of trend and interannual oscillatory variabilities of precipitation are then characterized and discussed in section 4, and a summary of the results follows in section 5.

2. Data and strategy

a. Database and preparation

The data used in this study are from the set, which contains daily precipitation records from 223 stations in the former Soviet Union for the period from January 1881 (or later) to December 1989, given by the Research Institute of Hydrometeorological Information in Obninsk, Russia, to the Carbon Dioxide Information Analysis Center of the Oak Ridge National Laboratory. Among the 223 stations, 102 are located in the Northern Eurasian sector (35°–135°E, 50°–70°N); 94 of the 102 stations have nearly complete records for the 1939–89 period (51 yr), with 37 of them having records for at least 90 yr (see Fig. 1, excluding the eight stations with shorter time series marked by crosses). The present study mainly focused on the 51-yr period; all records for the period before 1891 were not used, to avoid the unknown inhomogeneities prior to the installation of the Nipher shield, which increased precipitation measurements, especially during the cold season (Groisman et

TABLE 1. Some statistics measuring the goodness of fit of the multistate precipitation model to the observed daily precipitation at station 33 (see Fig. 1) being compared with those of a two-state model. Here, T is the total number of specific calendar months (e.g., total number of Aprils) without missing data during 1897–1989. Here, W is the total number of wet days in the T months; U and S denote the mean and standard deviation of daily precipitation (mm) on wet days. The subscripts "o," "m," and "2" denote statistics of the observed, multistate model, and two-state model simulated daily precipitation series, respectively.

	T	W_o	$W_m - W_o$	$W_2 - W_o$	U_o	$U_m - U_o$	$U_2 - U_o$	S_o	$S_m - S_o$	$S_2 - S_o$
Jan	75	996	7	32	0.59	0.00	0.02	0.62	−0.03	−0.02
Feb	77	808	31	28	0.63	0.03	0.07	0.75	−0.04	0.09
Mar	78	640	2	9	0.72	0.06	−0.07	0.97	0.02	−0.10
Apr	76	513	18	23	1.49	0.05	−0.08	2.04	0.03	−0.09
May	79	620	−40	−40	2.38	−0.12	−0.11	3.21	0.00	−0.03
Jun	79	790	42	−54	3.33	0.19	−0.19	3.99	−0.07	−0.23
Jul	77	746	26	29	4.46	0.18	0.25	6.00	−0.11	0.60
Aug	77	836	−53	−55	4.34	−0.09	0.11	5.57	−0.42	0.32
Sep	78	814	−55	−55	2.87	0.18	0.27	3.84	0.19	0.31
Oct	79	1114	−3	−5	1.57	0.02	0.03	2.55	−0.12	0.20
Nov	79	1193	−11	−24	1.02	0.05	0.05	1.59	0.07	0.05
Dec	78	1086	−6	−19	0.72	−0.01	0.03	0.86	−0.05	0.03

al. 1991). Throughout the record, daily precipitation is defined as the total amount of precipitation recorded during a 24-h period, with snowfall being converted to a liquid amount by melting the snow in the gauge.

In the dataset, there are months in which some daily precipitation records were missing for some station(s); missing data (if any) often occur in most days of a calendar month. During the 1939–89 period (18 628 days), the total number of missing daily records is less than 5% for most of the 102 stations, except stations 38 (5.9%), 98 (5.9%), 22 (6.5%), 31 (9.3%), 16 (10.3%), and 49 (18.3%) (see Fig. 1 for their locations). Under such circumstances, a stochastic multistate precipitation model has been developed to fill the gaps of missing data in the series.

For each of the 12 calendar months, weather states were classified in the following way (Yao and Ding 1990): dry days (daily precipitation < 0.1 mm) as state 0, the first wet day of every wet spell (i.e., consecutive days of daily precipitation being not less than 0.1 mm) as state 1, the second wet day as state 2, the nth wet day as state n, and so forth. The number of days of the longest wet spell at each site is finite, say S days. Thus, the historical records of weather at a site were classified into a finite number of states: $n = 0, 1, 2, \ldots, S$. For each such weather state n ($n < S$), there exist *only* two succession–transition possibilities: one is state $(n + 1)$, $n \rightarrow (n + 1)$; another is state 0, $n \rightarrow 0$ (i.e., the wet spell ends); while only one transition–succession possibility exists for the state S (when the longest wet spell is reached), that is, turning into a dry spell with probability $p[S \rightarrow 0] = 1$. (The case $n \rightarrow n$ can happen *only* when $n = 0$; such a case is already included in the case $n \rightarrow 0$.) From the historical records of daily precipitation for a specific calendar month at a site (months containing missing daily records were excluded here), all the above transition probabilities can be calculated, which represent the relevant occurrence process of precipitation. With these transition probabilities, a sequence of weather states delineating the precipitation occurrence process in the specific calendar month can be generated by Monte Carlo simulation. For each site, such simulation was carried out separately for each of the 12 calendar months.

Variation of precipitation amounts on wet days is characterized using the two-parameter gamma distribution. In terms of the two distribution parameters, α (the shape parameter) and β (the scale parameter), the mean precipitation amount (considering only wet days) is $\mu = \alpha\beta$, and the corresponding variance is $\sigma^2 = \alpha\beta^2$ (Wilks 1992). Again, separate pairs of precipitation amount parameters were defined and calculated for each calendar month; months containing missing daily data were excluded in these calculations.

Once the parameters representing the precipitation occurrence process (the transition probabilities) and precipitation amounts on wet days (the α and β) are calculated, generation of synthetic sequences of daily precipitation for the months of missing data is straightforward. Knowing the weather state, n, of the previous day (observed for the first simulation day and simulated for the others), the transition probability, $p[(n \rightarrow (n + 1)]$ $(n = 0, 1, 2, \ldots, S - 1)$, is compared to a newly generated uniform [0, 1] random number. A wet day [i.e., state $(n + 1)$, $(n + 1) \geq 1$] is simulated if the transition probability is greater than the random number; otherwise, a dry day (state 0) is simulated. If a wet day is simulated, a random precipitation amount is generated for this day using the appropriate gamma distribution. This interpolation scheme (a multistate model) considers the historical evolution of the weather states and the persistence and seasonality of precipitation, and was found to be able to represent precipitation processes well. For most locations, it was able to reproduce more realistic total number of wet days than does a commonly used model (a two-state model) in which the occurrence of precipitation is governed by a two-state, first-order stationary Markov train (e.g., Wilks 1992). As an example, Table 1 gives some statistics measuring the goodness of fit of the multistate model to the observed daily

precipitation series at station 33 (see Fig. 1 for its location), which are also compared with those of the two-state model.

After all gaps of missing data in the daily precipitation series were filled, series of monthly precipitation amounts were calculated from the daily precipitation series. Then, the monthly precipitation time series were corrected for biases of precipitation measurement due to gauge-type changing (from old Nipher shielded gauges to the new Tretiyakov gauges) and for changes in observing procedures, using the K_1 and K_3 correction coefficients of Groisman et al. (1991) for the relevant station. These corrections are indispensable for climate change studies, since the biases are too big to be disregarded (cf. Fig. 9). The corrected monthly precipitation time series were then used in the present study.

b. Strategy

First of all, spatial principal component analysis (PCA) was performed on the dataset of monthly precipitation (without removing the annual cycle) for the 94 stations (see Fig. 1, excluding the eight stations marked by crosses) for a 51-yr period (1939–89). The first few leading spatial eigenvectors (S-EOFs) and their associated spatial principal components (S-PCs) represent the most important part of the original variability of the precipitation and hence were retained for further analyses (cf. section 3).

Then, both uni- and multivariate singular spectrum analyses were applied in this study. Singular spectrum analysis (SSA) is a powerful form of PCA of the lag-correlation structure of time series. Univariate singular spectrum analysis (USSA) aims first to solve the eigenvalue problem of the lag–autocovariance matrix of a single time series, while multivariate (multichannel) singular spectrum analysis (MSSA) aims first to solve the eigenvalue problem of a block-Toeplitz matrix that contains the lag–cross-covariance matrices of the L variates, where L ($L \geq 2$) is the number of variates (cf. appendix; Wang et al. 1996a; Plaut and Vautard 1994). The maximum time lag considered in SSA is called window length (M, measured in number of sampling intervals).

The eigenvectors and associated principal components derived by USSA are usually referred to as temporal EOFs (T-EOFs) and temporal PCs (T-PCs), respectively. Performing USSA, one can identify signals of significant trends, if any, and periodic components of periods greater than the maximum time lag considered (i.e., M sampling intervals) and separate them from higher-frequency and noise components in the single time series. This property of SSA was used in the present study to filter out high-frequency and random components from leading S-PCs, without reducing the sampling rate. More specifically, USSA with a window length $M = 13$ months was performed on each of the retained leading S-PCs of precipitation separately, to separate slower-than-annual variations from annual and higher-frequency components.

To reveal the spatial–temporal structures of low-frequency variabilities of the precipitation, MSSA analyses with window lengths of 120, 96, and 84 months (M = 120, 96, 84) were carried out on the USSA-identified low-frequency components (multiple time series) of the leading S-PCs. By performing MSSA, one obtains sequences of spatial modes (EOFs), with each spatial mode corresponding to a time lag τ ($\tau = 0, 1, \ldots, M - 1$ sampling intervals). Such eigenvector sequences represent both spatial and temporal variabilities and thus are referred to as spatial–temporal EOFs (ST-EOFs) and the relevant PCs are called spatial–temporal PCs (ST-PCs). MSSA corresponds to oscillatory components by forming pairs of ST-EOFs, with each pair corresponding to one or two of the dominant frequencies present; a pair of oscillatory ST-EOFs or the associated ST-PCs are in quadrature with each other (Wang et al. 1996a; Plaut and Vautard 1994). The oscillatory pairs may be identified tentatively by their nearly equal eigenvalues (Vautard and Ghil 1989). In practice, a pair of eigenelements (k, $k + 1$) was selected as an oscillatory pair under the following conditions.

1) The frequencies f_k and f_{k+1}, corresponding to the maximum spectral values of ST-PC$_k$ and ST-PC$_{k+1}$, satisfied the inequality $2M|f_k - f_{k+1}| < 0.75$ (Vautard et al. 1992), so that the pair of ST-PCs were suspected to share the same frequency. The power spectra of the ST-PCs were estimated by maximum entropy method based on the formulation of Barrodale and Erickson (1980).

2) The lags at which cross correlations between ST-PC$_k$ and ST-PC$_{k+1}$ were maximized and statistically significant were equal to one-quarter of the apparent period of the eigenelements (cf. Table 2). The significance of the cross-correlation maxima were determined by comparing the maxima with the range of correlations at the same lags in surrogate ST-PCs obtained from pure red-noise realizations. The surrogate ST-PCs were generated by projecting 1000 red-noise series (with the same length, number of channels, observed variance, and lag-one correlations as the relevant L-channel variables) onto the suspected oscillatory pair of ST-EOFs (Dettinger et al. 1995). Readers are referred to Wang et al. (1996a), Plaut and Vautard (1994), and Vautard et al. (1992) for a more detailed description of MSSA and USSA.

3. Dominant spatial modes and slower-than-annual components of precipitation

The spectrum of normalized eigenvalues representing the fractions of the total variance captured by the first 35 pairs of the eigenelements (S-EOFs and S-PCs) of the monthly precipitation is shown in Fig. 2. The gap between the eigenvalues for S-EOF10 and S-EOF11 is about 1.6 times the estimate of their sampling error

TABLE 2. Trend and oscillatory components of precipitation over the Northern Eurasian sector identified in MSSA analyses with three different window lengths. The variance fraction is percentage relative to the total slower-than-annual variability. All the correlations here are significantly (at 95% level) higher than the relevant red-noise correlations. Lags are positive when ST-PC$_k$ leads ST-PC$_{k+1}$, and negative otherwise. The two successive antisign correlation maxima should be half the corresponding quasi cycle apart (cf. the last paragraph of section 2b).

Window lengths (months)	Components (orders of ST-PCs)	Variance fractions	Trend or quasi periods (yr)	Maximal lag–cross correlations between the oscillatory pair of ST-PCs at the indicated lags
120	1	24.79%	trend	—
	2–3	21.07%	4.20–4.86	−0.6894 at 14 months
				0.6568 at −11 months
	8–9	5.33%	2.26	0.8356 at 8 months
				−0.8006 at −6 months
96	1	27.22%	trend	—
	2–3	23.94%	4.58–5.43	−0.7549 at 17 months
				0.5885 at −12 months
	8–9	5.25%	2.05–2.08	0.3528 at 6 months
				−0.5472 at −7 months
84	1	29.03%	trend	—
	2–3	27.00%	4.78–5.12	0.8434 at 18 months
				−0.6188 at −12 months
	6–7	6.97%	2.18–2.22	0.6741 at 7 months
				−0.8763 at −7 months

(North et al. 1982), whereas there is no gap between the error bars of the higher-order eigenvalues. Therefore, the first 10 S-EOFs and the associated S-PCs, which together account for about 72.2% of the total variance, were retained for further analyses.

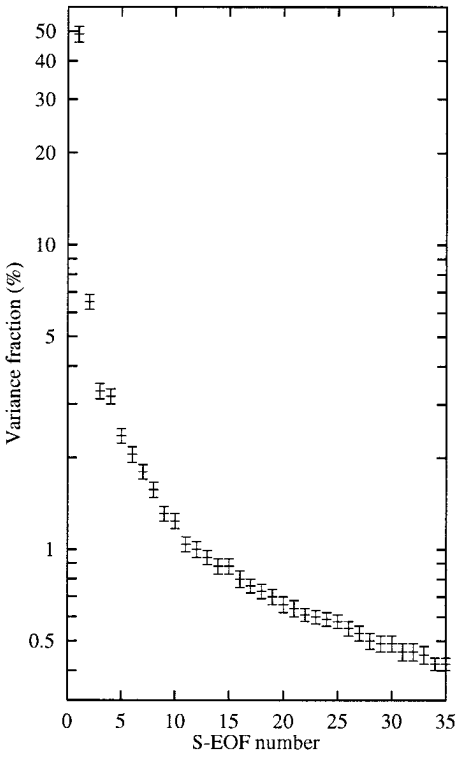

FIG. 2. Variances explained by the leading S-PCs and S-EOFs (in percentage of the total variance) of monthly precipitation (1939–89) over the Northern Eurasian sector. The vertical error bars are based on the estimate of eigenvalue sampling error proposed by North et al. (1982).

Singular spectrum analysis is typically successful in isolating periodic components of periods in the range (M/5, M). Also, robust trends, if any, and oscillatory components of periods longer than M (in number of sampling intervals) will be represented by some leading T-PCs and T-EOFs. In order to extract slower-than-annual components of precipitation variation, USSA with a window length $M = 13$ months was carried out on each of the 10 leading S-PCs, separately. Most of the precipitation variability associated with the seasonal cycle was represented by the first pair of T-PCs (T-PC1 and T-PC2) of the S-PC1, with T-PC3 and T-PC4 representing the biannual variation. Annual components were also found in the S-PC2, S-PC3, and S-PC4, represented by the first pair of T-PCs, but these are negligible when compared with those identified in the S-PC1. The most dominant slower-than-annual components (including trend, if any, and oscillatory components) turned out to exist in the S-PC1 and S-PC2, being represented by the T-PC5 of the S-PC1 and by the T-PC3 of the S-PC2. These slower-than-annual components were found to be significant at the 99% confidence level in the Kendall test of randomness. At the 99% confidence level, no significant slower-than-annual components were identified for the S-PCs of orders 3–10. Therefore, the first two leading S-PCs and the associated S-EOFs were retained for further analyses aiming at the slower-than-annual variability.

Figure 3 shows the first two S-EOFs, the most dominant spatial modes of the precipitation. The S-EOF1 is positive everywhere, with the highest values in the southeastern part of the Northern Eurasian sector and some relatively high values in Western Siberia (an east–west band around 60°N). This spatial mode resembles the spatial distribution of the long-term mean annual

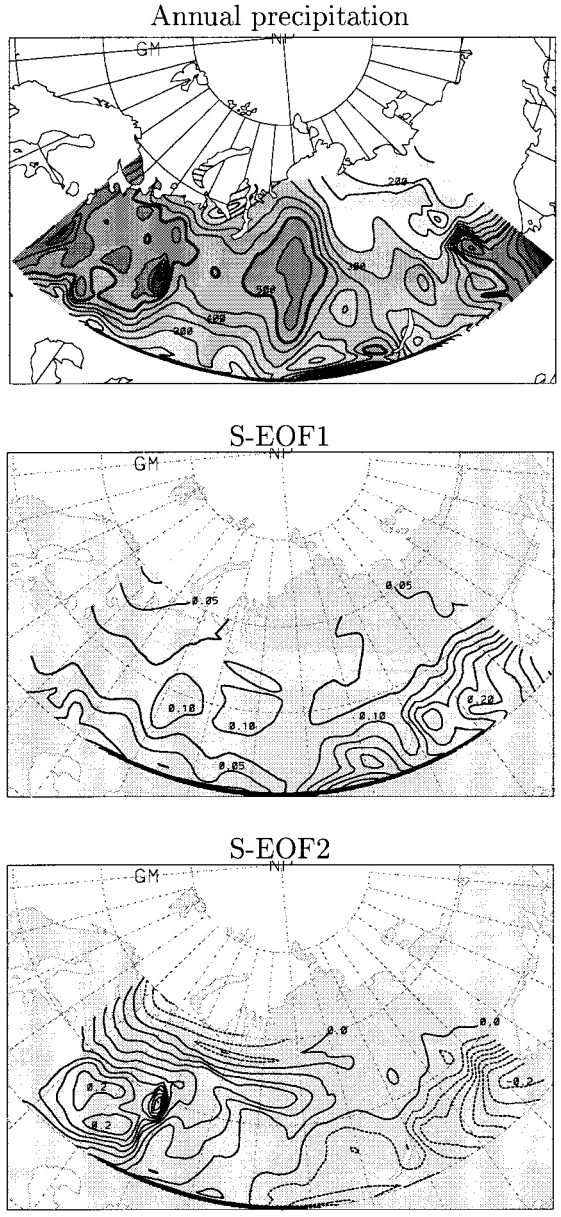

FIG. 3. The most dominant spatial modes (S-EOFs) of monthly precipitation and the spatial distribution of long-term mean annual precipitation over the Northern Eurasian sector. The contour interval is 0.025 for the S-EOFs and 50 mm for the annual precipitation map. Dashed where negative. The bold lines are 0.075 contours for S-EOF1, zero contours for S-EOF2, and 500-mm contours for the annual precipitation map.

precipitation over the sector (also shown in Fig. 3), representing the long-term mean pattern of precipitation. Together with the associated S-PC1, this mode captures about 49% of the total variability of monthly precipitation. The S-EOF2 represents the out-of-phase variation between the southeastern part (around and east of Lake Baikal) and most of the western half of the Northern Eurasian sector, accounting for about 6.5% of the total variance.

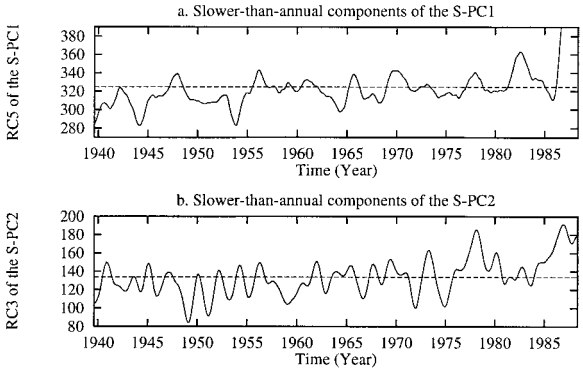

FIG. 4. Slower-than-annual components of the leading S-PCs of monthly precipitation over the Northern Eurasian sector derived in the USSA analyses with a window length of 13 months.

With the reconstruction technique developed by Vautard et al. (1992; cf. appendix), time series delineating variations of some interested frequencies can be obtained from the T-PC(s) and T-EOF(s) corresponding to those frequencies. Such time series are referred to as reconstructed components and are directly comparable with the retained leading S-PCs. Following this technique, time series representing low-frequency (slower-than-annual) variations in each of the two leading S-PCs were estimated (from the T-PC5 and T-EOF5 of the S-PC1, and from the T-PC3 and T-EOF3 of the S-PC2, respectively). These time series are actually low-pass-filtered leading S-PCs. As can be seen from Fig. 4, interannual variations are apparent in both time series; also, both series appeared to have trends. These two time series were then subject to MSSA analyses to characterize the spatial–temporal structures of the low-frequency variabilities of precipitation. However, the 14 data values at the two ends of the time series were discarded, to avoid the possible phase shift (Vautard et al. 1992; Wang et al. 1996a,b) there caused by the reconstruction technique (cf. appendix).

4. Spatial–temporal structures of precipitation low-frequency variabilities

In order to reveal the spatial–temporal structures of low-frequency variabilities of precipitation, MSSA was applied to the bivariate time series (shown in Fig. 4) representing major low-frequency (slower-than-annual) variations of the precipitation. Since SSA is typically successful in isolating oscillatory components of periods in the range ($M/5$, M), the window length M should be selected carefully. In order to focus on the interannual timescales (2–10 yr), a window length of 120 months ($M = 120$) was chosen for the first MSSA analysis. Results from the analysis indicate that the first spatial–temporal principal component (ST-PC1) has a notable upward trend, while pairs of ST-PCs 2 and 3 and 8 and 9 appeared to represent oscillatory variations with periods of about 4–5 and 2.26 yr, as listed in Table 2.

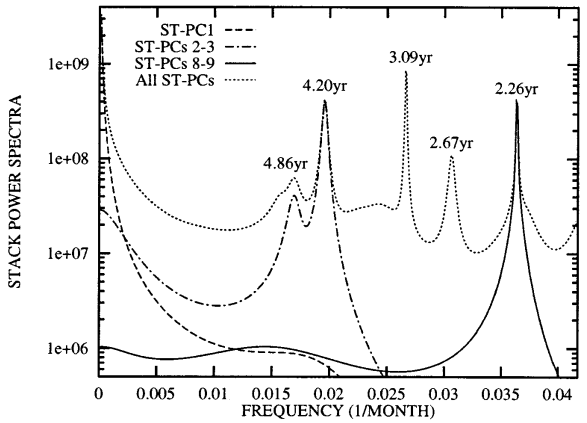

FIG. 5. Maximum entropy spectra (MES) of the indicated ST-PCs of low-frequency components of precipitation variation over the Northern Eurasian sector.

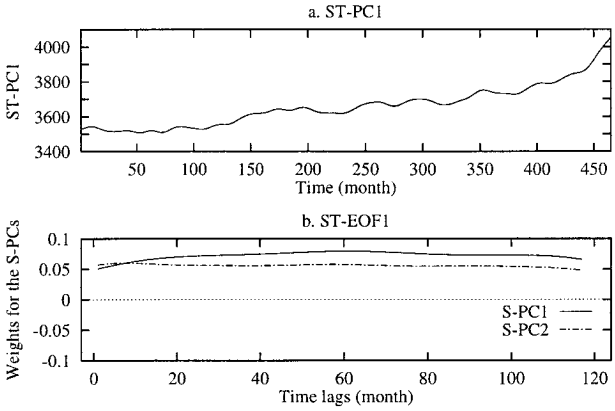

FIG. 6. The ST-PC1 and the associated ST-EOF1 of the low-frequency variations of precipitation over the Northern Eurasian sector, derived in the MSSA analysis with a window length of 120 months.

Maximum entropy spectra of the oscillatory pairs of ST-PCs (stack power spectra) are shown in Fig. 5, together with the stack spectra of all the ST-PCs. No oscillatory pairs of ST-PCs were found to be associated with the spectral peaks at 3.09 and 2.67 yr shown in Fig. 5.

In order to further examine the robustness of the trend and periodicities identified, to eliminate artificial results, MSSA analyses with window lengths of 96 and 84 months ($M = 96, 84$) were also carried out on the bivariate time series. The ST-PC1 in both MSSA analyses again turned out to represent a notable upward trend; also, the 4–5-yr and quasi-biennial periodicities were again found to be robust in both analyses (see Table 2), and no other periodicities were reproducibly found to be robust. The peaks at 3.09 and 2.67 yr (see Fig. 5) disappeared in both MSSA analyses and hence were suspected to be spurious. Furthermore, we randomly resampled the bivariate time series, destroying their inherent structure and thus creating random bivariate series with the same data values, and hence with the same mean and variance; then, we performed the same SSA analyses on the resampled series. As expected, we found neither trend nor periods from the randomly resampled series. This corroborates that the trend and the 4–5-yr and quasi-biennial periods are inherent features of the original bivariate time series.

Thus, we came to the conclusion that the trend and the 4–5-yr and quasi-biennial periodicities are inherent low-frequency variabilities of precipitation over the Northern Eurasian sector. The spatial–temporal structures of the trend components can be delineated by the ST-PC1 and ST-EOF1, while those of the oscillatory variabilities can well be represented by the corresponding pairs of ST-PCs and ST-EOFs derived in the first MSSA analysis. These will be discussed in the following sections.

a. Spatial–temporal structures of the precipitation trend

As shown in Fig. 6, the ST-PC1 possesses a notable upward trend. The associated ST-EOF1 consists of weights of this trend component for each of the two S-PCs. In other words, each of the S-PCs obtained its trend component from applying the corresponding weights to the ST-PC1 (cf. appendix). As can be seen in Fig. 6, the weights are positive for both S-PCs, indicating that the upward trend represented by the ST-PC1 is to be translated into an upward trend for both the S-PC1 and S-PC2. Figure 7 shows the trend components of the leading S-PCs (denoted as TCs), as estimated from the ST-PC1 and ST-EOF1 derived in the MSSA analysis with $M = 120$ months. The parts of the series corresponding to the periods before 1950 and after the summer of 1977 were not shown, because those values might be inaccurate due to the reconstruction procedure (cf. appendix).

According to the property of PCA, the trend com-

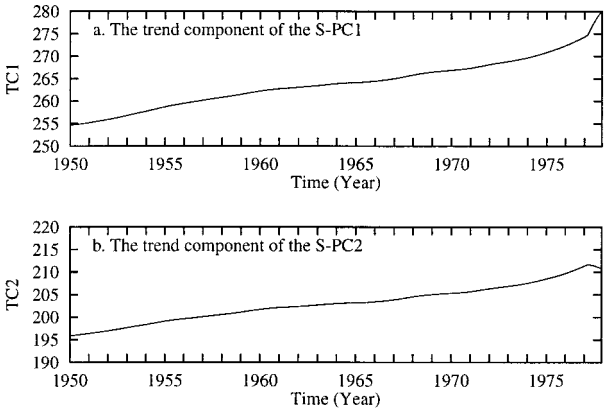

FIG. 7. The TCs of the leading S-PCs of monthly precipitation over the Northern Eurasian sector, as estimated from the ST-PC1 and ST-EOF1 derived in MSSA with a window length of 120 months.

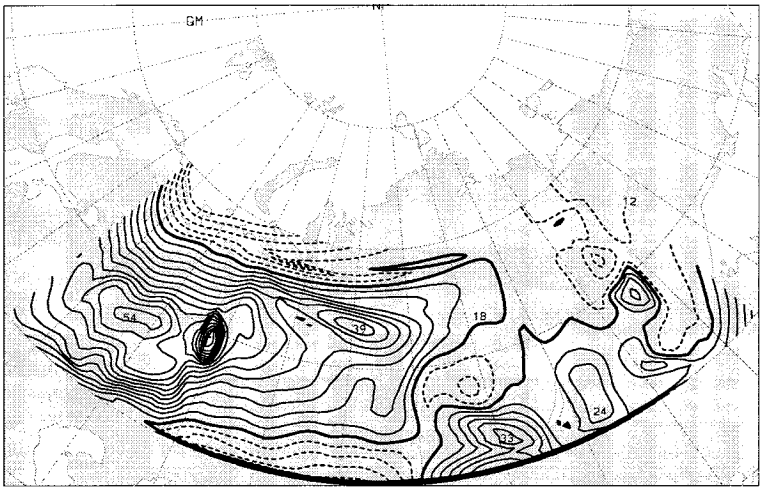

FIG. 8. Increases of annual precipitation (mm) over the Northern Eurasian sector during the 28-yr period from August 1951 to July 1978, as estimated from the ST-PC1 and ST-EOF1 derived in the first MSSA analysis ($M = 120$ months). The contour interval is 3 mm. The bold lines indicate the 18-mm contours, thin solid lines indicate contours above 18 mm, and dashed lines, below 18 mm.

ponent of space–time-dependent series of the precipitation can be estimated as

$$\mathrm{PT}(x, t) = \mathrm{S\text{-}EOF1}(x) \times \mathrm{TC1}(t) + \mathrm{S\text{-}EOF2}(x) \times \mathrm{TC2}(t),$$

where S-EOFk ($k = 1, 2$) are the leading S-EOFs, TCk are the trend components of the S-PCk (shown in Fig. 7), and x and t are location and time indices, respectively. An upward (downward) trend of S-PC is translated into precipitation increases (decreases) in those regions that have positive values of the associated S-EOF and decreases (increases) where the values of the S-EOF are negative. Therefore, the upward trend TC1 (Fig. 7) indicates that increases of precipitation occurred everywhere in the Northern Eurasian sector, being most notable in the southeastern part, that is, in the regions around and east of Lake Baikal (cf. S-EOF1 in Fig. 3). Likewise, the upward trend TC2 (Fig. 7) represents increases of precipitation in the western half of the sector and decreases in the southeastern part (cf. S-EOF2 in Fig. 3). Thus, the increase of precipitation is most notable in the western half of the Northern Eurasian sector, where the upward trend represented by the S-PC2 and S-EOF2 reinforces the upward trend represented by the S-PC1 and S-EOF1; it is less apparent in the southeastern part, because the downward trend represented by the S-PC2 and S-EOF2 partly cancels the upward trend represented by the S-PC1 and S-EOF1 over that region. Also, trend components are less noticeable over the Middle Siberian Plateau (Sredne-Sibirskoye Ploskogor'ye) and the region eastward, where the values of leading S-EOFs are smaller.

Based on the space–time-dependent trend (monthly) series PT(x, t), the differences of the annual precipitation between the year from August 1977 to July 1978 and the year from August 1950 to July 1951 [before August 1950 and after July 1978, the values of the trend series PT(x, t) might be biased due to the reconstruction procedure] were calculated and mapped in Fig. 8. Apparently, precipitation increases appeared to happen over the entire Northern Eurasian sector during the 28-yr period from August 1951 to July 1978. The largest increases of annual precipitation occurred in the southwestern part of the Northern Eurasian sector, the south-flowing Volga and Ural River basins, with increases of about 40–66 mm over the 28-yr period (1.4–2.4 mm yr^{-1} on the average). The second largest increases appeared in Western Siberia, the Ob and Irtysh River basins (approx. 18–40 mm 28 yr), and in the northwestern part, the Pechora and North Dvina River basins (approx. 15–35 mm 28 yr^{-1}), whereas, a slight upward trend (0.2–0.7 mm yr^{-1}) appeared in the eastern half of the sector (the Yenisey–Lena River basins). These corroborate the aforementioned features of the spatial structure of precipitation increases over the Northern Eurasian sector; also they are in agreement with Groisman's (1991) conclusions drawn from investigating areal mean annual precipitation over the regions.

It should be noted that the above trend components were extracted from the space–time-dependent series of monthly precipitation for the 1939–89 (51 yr) period. However, an upward phase of quasi-century periodicity could appear as an upward trend in a time series of 51-yr length. In order to distinguish the two possibilities, series of 10-yr moving averages of monthly precipitation were calculated and drawn. These moving average series, partly shown in Fig. 9, exhibited that notable increases of precipitation occurred in the Northern Eurasian sector during the last century, especially in the northwestern part, the North Dvina and Pechora River

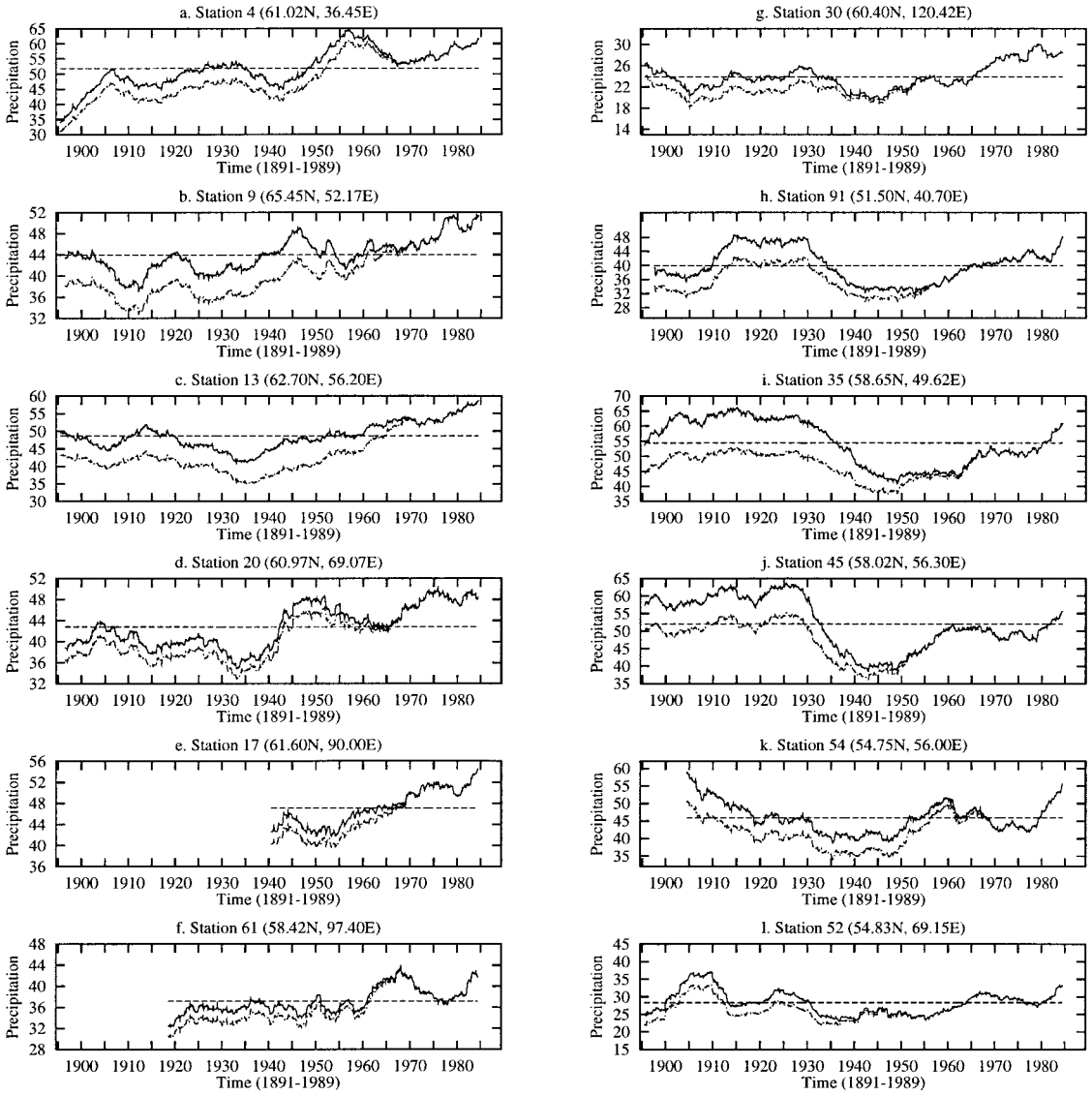

FIG. 9. The 10-yr moving average series of monthly precipitation (mm) at the indicated stations (see Fig. 1 for their locations) in the Northern Eurasian sector (dashed lines indicate series before the correction of biases of precipitation measurement).

basins (cf. Figs. 9a–c), and in Western Siberia, the Ob River basin (cf. Fig. 9d). Also, it can be seen that the increases of precipitation appeared to be more apparent during the last few decades. However, the notable increases of precipitation over the southwestern part (the Volga and Ural River basins) during the last half century appeared to be due at least in part to the upward phase of some quasi-century periodicity, since precipitation there turned out to possess such periodicity, as indicated by the series shown in Figs. 9h–l, with the last half century (1939–89) being the upward phase.

In order to check if the increase of precipitation possesses seasonalities, series of 10-yr moving averages of seasonal precipitation were also calculated for each of the four seasons [January–March (JFM), April–June (AMJ), July–September (JAS), and October–December (OND)] of the year, and some representative ones are shown in Fig. 10. Generally, in the northwestern part of the Northern Eurasian sector, the precipitation increase is more apparent during the cold seasons, especially during OND (cf. Figs. 10a–c), while in the eastern part, it appeared to be equally or more noticeable during summer (cf. Figs. 10e,f).

b. Spatial–temporal structures of precipitation oscillatory variabilities

On the interannual timescales, signals of 4–5-yr and quasi-biennial oscillations have been found in the space–time-dependent series of monthly precipitation over the Northern Eurasian sector. These oscillatory variabilities together account for about 5% of the total non-

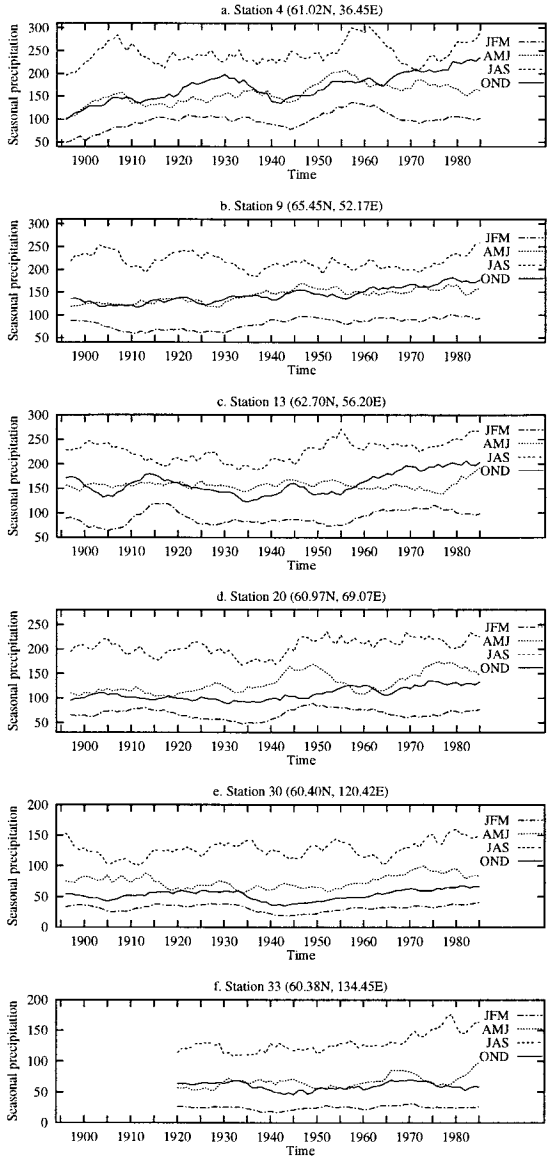

FIG. 10. The 10-yr moving average series of seasonal precipitation (mm) (biases corrected) at the indicated stations in the Northern Eurasian sector.

seasonal variance of monthly precipitation and can well be represented by the oscillatory pairs of ST-PCs 2 and 3 and 8 and 9 and the associated ST-EOFs derived in the MSSA analysis with $M = 120$ months (cf. Table 2 and Fig. 5).

Using the reconstruction technique developed by Vautard et al. (1992), the 4–5-yr oscillatory components of the S-PCs can be estimated from the pair of ST-PCs 2 and 3 and the associated ST-EOFs; the quasi-biennial oscillatory components, from the ST-PCs 8 and 9 and the corresponding ST-EOFs. Such oscillatory components (reconstructed series) of the S-PCs are shown in Figs. 11 and 12, respectively, excluding the 134 (i.e., 120 + 14) data values at the two ends of the reconstructed series to avoid possible phase shift there (Vautard et al. 1992; Wang et al. 1996a, b). The 4–5-yr oscillatory variability was present in each of the two leading S-PCs, with larger amplitudes in the S-PC1, while the quasi-biennial oscillatory variability is almost equally strong in the two S-PCs, with smaller amplitudes during the 1955–65 period (cf. Figs. 12 and 14). Generally, the quasi-biennial signal is weaker than the 4–5-yr periodicity.

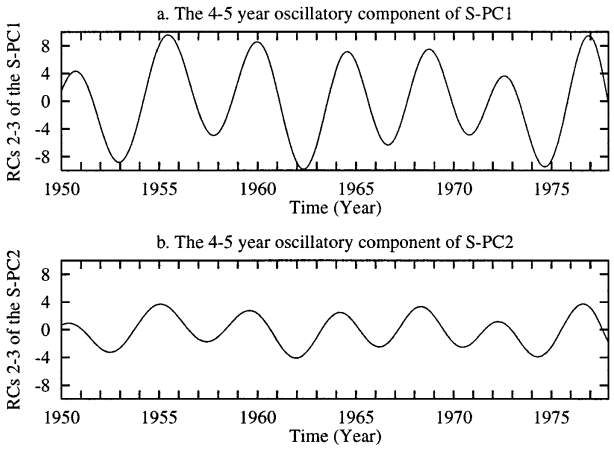

FIG. 11. The 4–5-yr oscillatory components of the indicated S-PCs of precipitation over the Northern Eurasian sector, as reconstructed from the oscillatory pair of ST-PCs 2–3 and the associated ST-EOFs derived in the first MSSA analysis ($M = 120$ months).

The space–time-dependent series of the oscillatory components can be obtained by summing the products of the relevant reconstructed oscillatory components of the S-PCs and the associated S-EOFs. Such space–time-dependent (reconstructed) series represent the spatial–temporal structures of the oscillations, like the corresponding ST-EOFs. Mapped in Fig. 13 are the differences of the oscillatory components of precip-

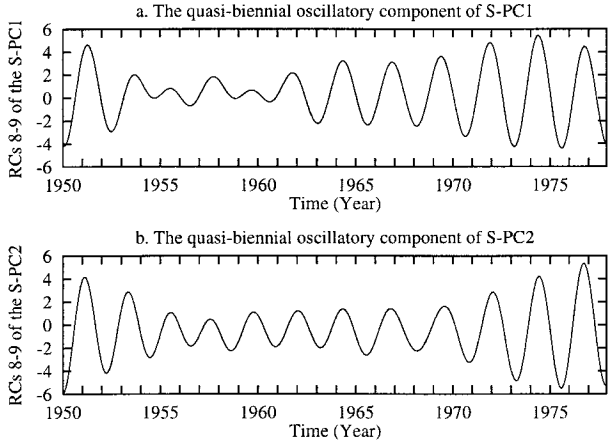

FIG. 12. Quasi-biennial oscillatory components of the indicated S-PCs of precipitation over the Northern Eurasian sector, as reconstructed from the oscillatory pair of ST-PCs 8–9 and the associated ST-EOFs derived in the first MSSA analysis ($M = 120$ months).

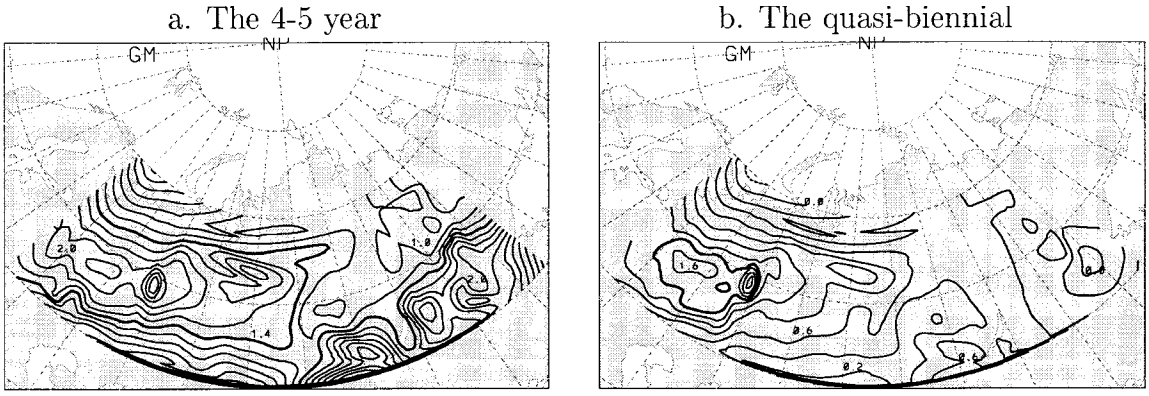

FIG. 13. Differences of monthly precipitation reconstructions (mm) between the extreme high and low phases (opposite phases) of the oscillations. The extreme high and low phases were defined as the high and low peaks of (a) the 4–5-yr oscillatory component of the S-PC1 and (b) the quasi-biennial oscillatory component of the S-PC2. The contour interval is 0.2 mm. The bold lines indicate the 1.4-mm contours and the dashed lines, negative values. Note that these indicate a sort of long-term mean (1952–76) mean magnitude of the oscillations. The amplitude of oscillation may vary from cycle to cycle (cf. Fig. 14).

itation between the opposite phases (extreme high and low phases, or high and low peaks) of the oscillations. The extreme high and low phases were defined as the high and low peaks of the 4–5-yr oscillatory component of the S-PC1, or of the quasi-biennial oscillatory component of the S-PC2. These maps actually manifest, on an average, the spatial patterns of the amplitudes of the oscillations. In addition, for stations 37, 46, 78, and 85 (located in the western, central, and eastern parts of the Northern Eurasian sector; cf. Fig. 1), the reconstructed series of precipitation deviations associated with each oscillation were presented in Fig. 14, showing representatively the amplitudes of the oscillations at different locations and the phase relationship between different parts of the Northern Eurasian sector.

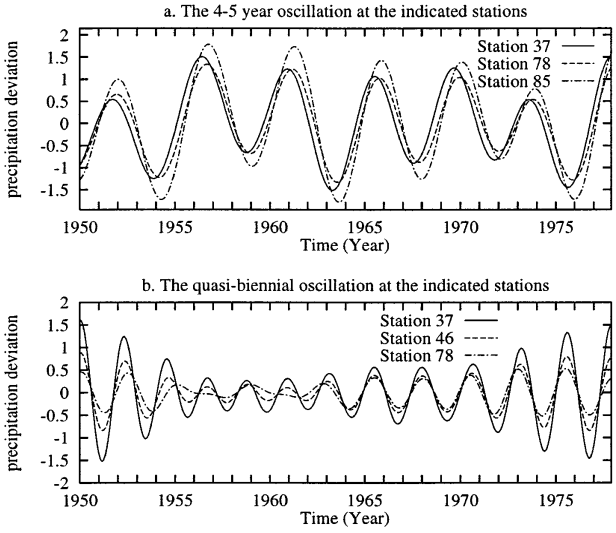

FIG. 14. Series of the indicated oscillatory components of monthly precipitation deviations (mm) at the indicated stations located in the western (station 37), the central (stations 46 and 78), and the easternmost parts (station 85) of the Northern Eurasian sector, respectively, being reconstructions from the corresponding reconstructed oscillatory components of the leading S-PCs and the associated S-EOFs.

As clearly shown in Fig. 13a, the 4–5-yr oscillatory variability is quite apparent over the whole sector and stronger in the southeastern and western parts. Figure 14a not only further demonstrates this spatial feature of the oscillation, but also shows that the 4–5-yr oscillation appeared to be associated with an eastward propagating wave motion: the phase of the oscillation in the western part (e.g., station 37) leads that of the eastern part (e.g., station 85) by about 4 months and that around Lake Baikal (e.g., station 78) by about 3 months.

Figure 13b shows that the quasi-biennial oscillation of precipitation is much stronger in the western half of the Northern Eurasian sector than in the eastern half, with the amplitudes reducing from the west to the east. This spatial feature of the quasi-biennial oscillation is further demonstrated in Fig. 14b. There is no apparent phase difference between stations in the western (station 37) and in the central (stations 46 and 78) parts of the Northern Eurasian sector.

5. Summary and discussions

Knowledge of precipitation variability, such as trends and periodicities, is useful for the understanding of the earth's climate system. The main contribution of this study is the detailed characterization of the spatial–temporal structures of trend and interannual oscillatory variabilities of precipitation over the north-flowing river basins in the Northern Eurasian sector, where changes in precipitation could have significant impacts on the global thermohaline circulation and hence on the climate of the earth. This was achieved by performing combinations of statistical analyses. Specifically, the dataset of monthly precip-

itation series derived for 94 stations in the North Eurasian sector for the 1939–89 period was compressed into 10 leading principal components (S-PCs) and the associated S-EOFs. Then, univariate singular spectrum analysis was performed on each of the 10 S-PCs, separately, to check for the slower-than-annual components of precipitation variation. As a result, the most dominant slower-than-annual components were found in the first two S-PCs. Thus, multivariate singular spectrum analysis was applied to the slower-than-annual component series of the two leading S-PCs, to analyze trends and interannual oscillatory variability of precipitation. Also, series of 10-yr moving averages of monthly and seasonal precipitation for the last century were calculated and used to examine the precipitation trend and its seasonality.

An upward trend was found in the precipitation series for the Northern Eurasian sector during the last half century. This trend was most notable in the northwestern part (the Pechora and North Dvina River basins) and in the middle-west part (the Ob and Irtysh River basins); the increase rate is about 0.5–1.5 mm yr^{-1}. It was much weaker in the eastern half of the sector (the Yenisey–Lena River basins), appearing as a slight upward trend of about 0.2–0.7 mm yr^{-1}. Moreover, the increases of precipitation appeared to be more apparent during the last few decades, especially in the North Dvina, Pechora, and Ob River basins. In addition, quite notable increases of precipitation (about 1.4–2.4 mm yr^{-1} on the average) were also found in the southwestern part—the Volga and Ural River basins; however, these increases appeared to be at least in part due to a significant quasi-century periodicity. Generally, the increases of precipitation in the western half of the sector were more notable during the cold seasons, while in the eastern part it appeared to be equally or more apparent during the summer. It should be stressed that the aforementioned upward trend of precipitation was identified from the precipitation series already corrected for the biases of precipitation measurement caused by the gauge-type change and changes in observing procedures.

On the interannual timescales, two quasi periodicities with periods of 4–5 and about 2.26 yr were identified from the precipitation series. The 4–5-yr oscillation was quite apparent over the entire Northern Eurasian sector, being stronger over the southeastern and western parts. It appeared to propagate eastward; the phases of this oscillation over the westernmost part of the sector precede those over the easternmost part by about 4 months. Theoretically, this propagative feature shall be useful for long-range forecasting. However, precipitation is highly variable, the variance involved in this propagative oscillatory variability is too small to be used practically for long-range forecasting. The quasi-biennial oscillation appeared to be more noticeable in the western half of the Northern Eurasian sector but less apparent over the eastern half; its amplitude was very weak during the 1955–65 period. Generally, this oscillation is even weaker than the 4–5-yr oscillation.

The 4–5-yr oscillation may be linked to the quasi-4-yr periodicity of El Niño–Southern Oscillation (ENSO), while the quasi-biennial oscillation is likely a manifestation of the tropospheric quasi-biennial variability. Using monthly observed precipitation data, Xie et al. (1996) identified significant relationships between ENSO and summer (June–August) precipitation over the Northern Siberian sector, while the standing feature of precipitation quasi-biennial oscillation (QBO) identified here is consistent with the essential mode of Northern Hemispheric sea level pressure (SLP) QBO reported by Trenberth and Shin (1984). By performing complex EOF analysis on seasonally averaged SLP anomalies, Trenberth and Shin concluded that the dominant mode of SLP QBO is essentially a standing wave pattern corresponding to a high-latitude zonal index with departures in the pressure of opposite sign in low and high latitudes. Through analyzing observed annual and monthly precipitation in the zone from 50°N to 50°S, Lau and Sheu (1988) found that the dominant global precipitation pattern fluctuates irregularly, with quasi-2- and quasi-4-yr (26 and 52 months) periods associated with Southern Oscillation, and that both oscillations possess apparent long-term amplitude modulations. They also found that there is significant nonlinear interaction between QBO and Southern Oscillation, suggesting that the QBO may be an even more fundamental long-term oscillation of the tropical ocean–atmosphere system than the Southern Oscillation. They argued that the ENSO-like cycles can arise from a basic quasi-2-yr oscillation in the tropical ocean–atmosphere system through its lagged effect from one year to the next, and that the long-term amplitude modulation of the QBO can also arise from this effect. Besides, they also suggested that the timing of the annual, and perhaps also of intraseasonal (30–60 day) oscillations at a critical phase of the QBO, may be important in influencing the subsequent evolution of the coupled ocean–atmosphere system.

Acknowledgments. We are grateful to Dr. Francis W. Zwiers for his helpful suggestions and constructive criticism on the first draft of this manuscript, and to both him and Dr. William D. Hogg for helpful discussions about interpolating the missing data in the daily precipitation series. We are indebted to Dr. Pavel Ya. Groisman for providing us with the coefficients for correcting the biases of precipitation measurement caused by the gauge-type change and changes in observing procedures, and to Dr. Byron Moldofsky (of the Cartography Office of the Department of Geography, University of Toronto) for providing us with the geographic coordinates for drawing the rivers shown in this paper. The research was supported by

a GEWEX grant from the Atmospheric Environment Service of Canada.

APPENDIX

Singular Spectrum Analysis

Let $X = \{X_{l,t};\ l = 1, 2, \ldots, L;\ t = 1, 2, \ldots, N\}$ ($L \geq 2$) denote an L-variate (or L-channel) time series with the same sample size N. With a selected window length M (measured in number of sampling intervals), MSSA aims to solve the eigenvalue problem of matrix T_X:

$$\mathbf{T}_X = \begin{pmatrix} T_{11} & T_{12} & \cdots & T_{1L} \\ T_{21} & T_{22} & \cdots & T_{1L} \\ \vdots & \vdots & \cdots & \vdots \\ T_{L1} & T_{L2} & \cdots & T_{LL} \end{pmatrix},$$

where $\mathbf{T}_{ll'}$ is the lag-covariance matrix between time series $X_{l,t}$ and $X_{l',t'}$ ($l, l' = 1, 2, \ldots L$) and

$$\mathbf{T}_{ll'} = \begin{pmatrix} C^{ll'}_{0,0} & C^{ll'}_{0,1} & \cdots & C^{ll'}_{0,M-2} & C^{ll'}_{0,M-1} \\ C^{ll'}_{1,0} & C^{ll'}_{0,0} & C^{ll'}_{0,1} & \cdots & C^{ll'}_{0,M-2} \\ \vdots & \ddots & \ddots & \ddots & \vdots \\ C^{ll'}_{M-2,0} & \vdots & C^{ll'}_{1,0} & C^{ll'}_{0,0} & C^{ll'}_{0,1} \\ C^{ll'}_{M-1,0} & C^{ll'}_{M-2,1} & \cdots & C^{ll'}_{1,0} & C^{ll'}_{0,0} \end{pmatrix},$$

where

$$C^{ll'}_{jj'} = \frac{1}{N - |j - j'|} \sum_{i=1}^{N-|j-j'|} X_{l,i} X_{l',i+j-j'};$$
$$j, j' = 1, 2, \ldots (M - 1)$$

is the lag-covariance between $X_{l,t}$ and $X_{l',\,t+\tau}$ with time lag $\tau = j - j'$. Note that the element $C^{ll'}_{j,j'}$ equals a constant so long as the absolute time lag $|j - j'|$ is a constant, no matter whether $j > j'$ or otherwise. Thus, $\mathbf{T}_{ll'}$ is a Toeplitz matrix—a matrix of elements constant along the upper-left to lower-right diagonals—and $\mathbf{T}_X$ is called a block-Toeplitz matrix. Solving eigenvalue problem of $\mathbf{T}_X$ results in time sequences of eigenvectors; each sequence, called an ST-EOF, is composed of M eigenvectors that correspond to time lags $\tau = 0, 1 \ldots, (M - 1)$, respectively, delineating the M-step time evolution of a spatial pattern, that is, a spatial–temporal structure. The principal component series associated with an ST-EOF, referred to as a spatial–temporal PC (ST-PC), is of length $N - M + 1$ (i.e., N minus the maximum time lag $M - 1$), which is $M - 1$ points shorter than the original time series $X_{l,t}$. In order to obtain component time series directly comparable with the original multivariate time series, Plaut and Vautard (1994) developed the reconstruction technique: corresponding to the kth sequence of eigenvectors (i.e., ST-EOF$_k$ = $\{E^k_{lj};\ j = 1, 2, \ldots M\}$), the reconstructed component RC$_k$ = $\{R^k_{lt}\}$ is given by

$$R^k_{lt} = \begin{cases} \dfrac{1}{t} \displaystyle\sum_{j=1}^{t} (A^k_{t-j} E^k_{lj}) & \text{when } 1 \leq t \leq M - 1, \\ \dfrac{1}{M} \displaystyle\sum_{j=1}^{M} (A^k_{t-j} E^k_{lj}) & \text{when } M \leq t \leq N - M + 1, \\ \dfrac{1}{N - t + 1} \displaystyle\sum_{j=t-N+M}^{M} (A^k_{t-j} E^k_{lj}) & \text{when } N - M + 2 \leq t \leq N, \end{cases}$$

where A^k_{t-j} is the kth ST-PC series. Such a multivariate time series R^k_{lt} has the same sample size and same number of channels as the original multivariate series $X_{l,t}$. However, note that the number of eigenvectors used to obtain the first $M - 1$ and the last $M - 1$ values of R^k_{lt} is less than M, which might cause a phase shift there (cf. Plaut and Vautard 1994).

When $L = 1$, the aforedescribed MSSA reduces to the USSA.

REFERENCES

Barrodale, I., and R. E. Erickson, 1980: Algorithms for least-squares linear prediction and maximum entropy spectral analysis, Part (I). Theory. *Geophysics,* **45,** 420–432

Barry, R. G., M. C. Serreze, J. A. Maslanik, and R. H. Preller, 1993: The Arctic sea ice–climate system: Observations and modelling. *Rev. Geophys.,* **31,** 397–422.

Bradley, R. S., H. F. Diaz, J. K. Eischeid, P. D. Jones, P. M. Kelly, and C. M. Goodess, 1987: Precipitation fluctuations over Northern Hemisphere land areas since the mid-19th century. *Science,* **237,** 171–175.

Dettinger, M. D., M. Ghil, and C. L. Keppenne, 1995: Interannual and interdecadal variability in United States surface-air temperatures, 1910–87. *Climate Change,* **31,** 35–66.

Diaz, H. F., R. S. Bradley, and J. K. Eischeid, 1989: Precipitation fluctuations over global land areas since the late 1800s. *J. Geophys. Res.,* **94,** 1195–1210.

Groisman, P. Ya., 1991: Data on present-day precipitation changes in the extratropical part of the Northern Hemisphere. *Greenhouse-Gas-Induced Climatic Change: A Critical Appraisal of Simulations and Observations.* M. E. Schlesiger, Ed., Elsevier, 297–310.

——, V. V. Koknaeva, T. A. Belokrylova, and T. R. Karl, 1991: Overcoming biases of precipitation measurement: A history of the USSR experience. *Bull. Amer. Meteor. Soc.,* **72,** 1725–1733.

Houghton, J. T., B. A. Callander, and S. K. Varney, Eds., 1992: *Climatic Change 1992—The Supplementary Report to the IPCC Scientific Assessment.* Cambridge University Press, 200 pp.

Lau, K.-M., and P. J. Sheu, 1988: Annual cycle, quasi-biennial oscillation, and Southern Oscillation in global precipitation. *J. Geophys. Res.,* **93**(D9), 10 975–10 988.

North, G. E., T. L. Bell, R. F. Cahalan, and F. J. Moeng, 1982: Sampling errors in the estimation of empirical orthogonal functions. *Mon. Wea. Rev.,* **110,** 699–706.

Plaut, G., and R. Vautard, 1994: Spells of low-frequency oscillations and weather regimes in the Northern Hemisphere. *J. Atmos. Sci.,* **51,** 210–236.

Rahmstorf, S., 1995: Bifurcations of the Atlantic thermohaline circulation in response to changes in the hydrological cycle. *Nature,* **378,** 145–149.

Trenberth, K. E., and W.-T. K. Shin, 1984: Quasi-biennial fluctuations in sea level pressures over the Northern Hemisphere. *Mon. Wea. Rev.,* **112,** 761–777.

Vautard, R., and M. Ghil, 1989: Singular spectrum analysis in nonlinear dynamics, with applications to paleoclimatic time series. *Physica D,* **35,** 395–424.

——, P. Yiou, and M. Ghil, 1992: Singular-spectrum analysis: A toolkit for short, noisy chaotic signals. *Physica D,* **58,** 95–126.

Vinnikov, K. Ya., P. Ya. Groisman, and K. M. Lugina, 1990: Empirical data on contemporary global climate changes (temperature and precipitation). *J. Climate*, **3,** 662–677.

Wang, X., J. Corte-Real, and X. Zhang, 1996a: Low-frequency oscillations and associated wave motions over Eurasia. *Tellus,* **48A,** 238–253.

——, ——, and ——, 1996b: Intra-seasonal oscillations and associated spatial-temporal structures of precipitation over China. *J. Geophys. Res.*, **101**(D14), 19 035–19 042.

Weaver, A. J., 1995: Driving the ocean conveyor. *Nature*, **378,** 135–136.

Wilks, D. S., 1992: Adapting stochastic weather generation algorithms fort climate change studies. *Climate Change*, **22,** 67–84.

Xie, P., B. Rudolf, U. Schneider, and P. A. Arkin, 1996: Gauge-based monthly analysis of global land precipitation from 1971 to 1994. *J. Geophys. Res.*, **101**(D14), 19 023–19 034.

Yao, Z.-S., and Y.-G. Ding, 1990: *Climatological Statistics* (in Chinese). China Meteorological Press, 954 pp.